Catoptric electrodes: transparent metal electrodes using shaped surfaces

Pieter G. Kik[1,2]

[1]*CREOL, The College of Optics and Photonics, University of Central Florida, 4000 Central Florida Blvd., Orlando, Florida 32816, USA*

[2]*Also with Physics Department, University of Central Florida, 4000 Central Florida Blvd., Orlando, Florida 32816, USA (kik@creol.ucf.edu)*

Received April 1, 2014; revised July 18, 2014; accepted July 20, 2014; posted July 21, 2014 (Doc. ID 209337); published August 22, 2014

An optical electrode design is presented that theoretically allows 100% optical transmission through an interdigitated metallic electrode at 50% metal areal coverage. This is achieved by redirection of light incident on embedded metal electrode lines to an angle beyond that required for total internal reflection. Full-field electromagnetic simulations using realistic material parameters demonstrate 84% frequency-averaged transmission for unpolarized illumination across the entire visible spectral range using a silver interdigitated electrode at 50% areal coverage. The redirection is achieved through specular reflection, making it nonresonant and arbitrarily broadband, provided the electrode width exceeds the optical wavelength. These findings could significantly improve the performance of photovoltaic devices and optical detectors that require high-conductivity top contacts.

OCIS codes: (310.7005) Transparent conductive coatings; (040.5160) Photodetectors; (240.6680) Surface plasmons.
http://dx.doi.org/10.1364/OL.39.005114

Shadowing by electrical contacts on photodetectors is a major cause of signal loss. This is especially true in metal–semiconductor–metal (MSM) ultraviolet detectors, where short carrier recombination lengths and shallow absorption depths necessitate the use of closely spaced counter-electrodes. In order to achieve high device speed, these closely spaced contacts must have low resistance, typically achieved by implementing wide contacts. These factors result in a large fraction of the detector surface being covered by metal, causing severely reduced optical transmission. One approach to avoid these losses involves the use of transparent conductive materials, including indium tin oxide, aluminum-doped zinc oxide, graphene, and many others. An alternative approach is the use of relatively open random networks of good conductors such as carbon nanotubes, copper nanowires, and silver nanowires. Finally, surface-plasmon-assisted methods have been considered, including the use of periodically patterned electrodes resulting in plasmon-enhanced extraordinary transmission [1–3] and patterned surfaces exhibiting a plasmonic Brewster angle [4–6]. The present study introduces a new approach for achieving highly transparent electrodes that uses common materials, is nonresonant, does not required nanoscale patterning, and can operate at frequencies ranging from the near-ultraviolet to the far infrared. The approach relies on redirection of light incident on an embedded metallic interdigitated electrode toward angles beyond the angle for total internal reflection (TIR), and in a ray tracing analysis allows for 100% transmission at 50% metal coverage.

The presented approach is inspired by the *Cassegrain telescope* design [Fig. 1(a)] which transmits a large fraction of power incident on a curved primary mirror using an on-axis secondary mirror that focuses the incident light through an aperture in the primary mirror. Figure 1(b) shows an interdigitated electrode on a photodetector, illuminated at normal incidence (blue arrows). The large metal coverage in this example results in ~50% transmission loss due to reflection (green arrows) and optical absorption. To improve the detector response one could attempt to reclaim light reflected by the electrodes and return it to the electrode gap using an approach similar to the Cassegrain telescope as shown in Fig. 1(c). This could be achieved by covering the electrode with a dielectric layer that is index-matched to the substrate and defining a secondary reflector above the electrode gap. Although light incident onto the sculpted electrode lines is now focused onto the secondary reflector and redirected toward the electrode gap, the secondary reflector itself introduces substantial reflection loss. To overcome this problem the proposed approach uses

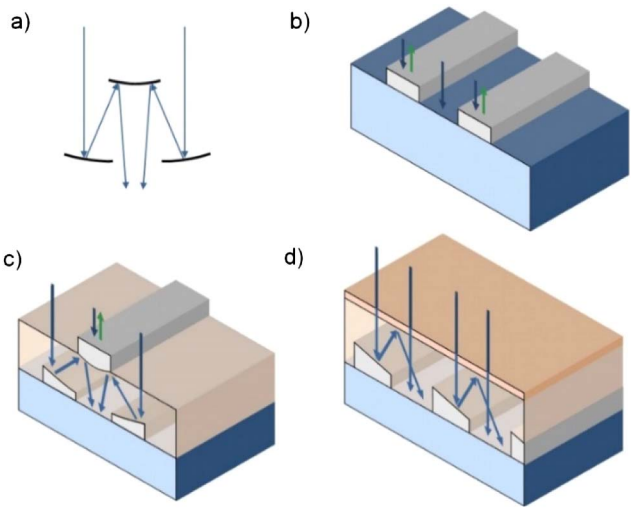

Fig. 1. (a) Cassegrain telescope design. (b) Cross section of an interdigitated electrode showing incident light (blue arrows) and reflection loss (green arrows). (c) Embedded electrode structure using a Cassegrain-like light gathering approach, showing collection of light incident on the electrodes as well as surface reflection loss by the secondary mirror. (d) Catoptric electrode consisting of sculpted electrode lines covered with an index-matching layer and an antireflection coating.

TIR to achieve redirection of light reflected by the electrodes, obviating the need for a metallic secondary reflector in the beam path. Due to the similarity of this approach to the catoptric telescope design, in the following it will be referred to as a "catoptric electrode."

Figure 1(d) shows a simple implementation of this approach, where the electrodes are embedded in a cover layer that is index-matched to the substrate and covered with an antireflection coating. Adjacent electrode lines have a top surface inclined at an angle θ greater than half the TIR angle θ_{TIR} of the cover layer. Incident light that strikes the tilted electrode is reflected specularly to an angle greater than θ_{TIR} followed by complete reflection toward the electrode gap where it is fully transmitted into the substrate. Note that this approach does not intrinsically rely on diffractive effects nor on a specific polarization of the incident light, implying the feasibility of broadband polarization-independent transmission enhancement.

To illustrate the conditions that allow enhanced transmission when using inclined electrode lines, Fig. 2(a) shows an example structure with electrode width W, periodicity P, and the distance D from the electrode to the top of the cover layer. The cover layer is assumed to be antireflection coated. A ray tracing analysis shows that at 50% metal coverage ($W = 0.5$ P), 100% transmission can be achieved when $D = 0.25 \times (\mathrm{Cot}(2\theta) - \mathrm{Tan}(\theta)) \times P$ where θ should exceed $\theta_{\mathrm{TIR}}/2$, assuming perfect metal electrodes. To illustrate how 100% transmission is achieved in this structure, the path of a light beam incident entirely on the left electrode is highlighted in red for a case where $\theta = 15°$ and $D = 0.366$ P. In order to achieve TIR at the reflected angle of 30° the cover layer index must exceed $n_{\mathrm{cov}} \geq 2$, but otherwise there are no intrinsic limitations on the refractive index of the substrate and cover layer. Under these conditions the entire beam incident onto the metal electrode is seen to reach the substrate after a maximum of three reflections. In this idealized geometrical example the actual thickness of the electrodes is not important, since light projected into the electrode gap will continue to reflect at the electrode sides until it reaches the substrate. Figure 2(b) shows the minimum allowed electrode tilt angle $\theta_{\mathrm{min}} = \theta_{\mathrm{TIR}}/2$ (green line) as a function of cover refractive index. The corresponding required cover layer thickness for achieving 100% transmission is included (blue solid line) expressed in relative units D/P. Note that for common refractive index values between 1.5 and 4 complete transmission can be achieved with cover layer thickness values less than the electrode spacing, demonstrating that this approach can be implemented in compact structures. Similar results are obtained when the electrode tilt is $1.2 \times \theta_{\mathrm{min}}$ (dashed line) and $1.4 \times \theta_{\mathrm{min}}$ (dotted line). The presented approach can be scaled virtually arbitrarily, within electrode tilt angular limits set by the refractive index of the substrate and cover layer, and is not intrinsically wavelength or polarization dependent.

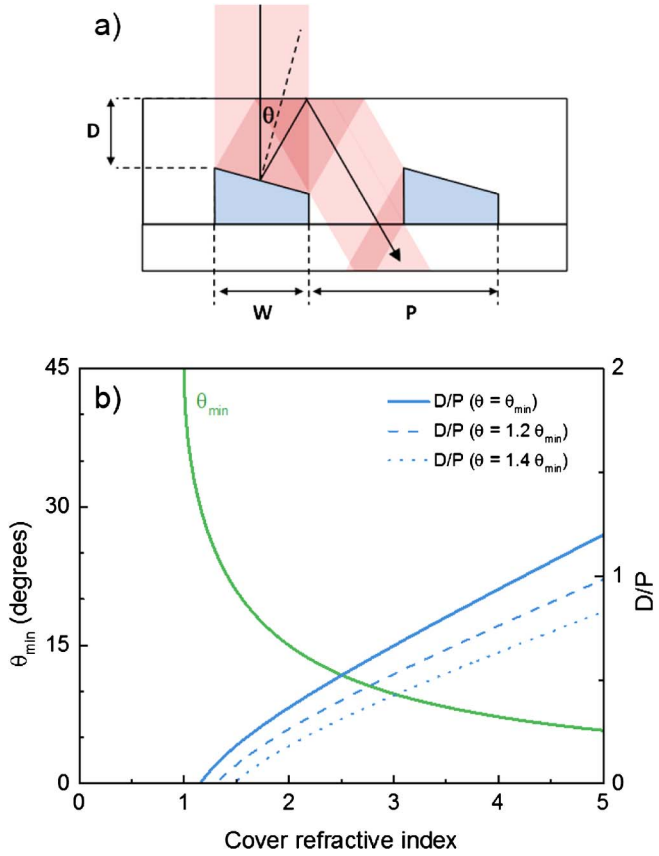

Fig. 2. (a) Cross section of a catoptric electrode with 50% metal areal coverage and a surface tilt of 15° showing complete transmission of all light incident on the metal electrode area. (b) Minimum electrode surface tilt to achieve total internal reflection (green line) and optimum scaled cover layer thickness D/P necessary for 100% transmission at a surface tilt equal to the minimum tilt (solid blue line) and at a surface tilt 20% (dashed line) and 40% (dotted line) above the minimum surface tilt.

To analyze the viability of the approach in realistic electrode structures, numerical simulations were carried out based on the frequency domain finite integration technique. Figure 3(a) shows a snapshot of the electric field distribution E_y under normal incidence TE illumination (electric field parallel to electrode) at $\lambda = 417$ nm of an interdigitated silver [7] catoptric electrode on a substrate with refractive index $n = 2$ embedded in an index-matched layer covered with an antireflection coating ($n = 1.41$, thickness 88 nm) for $\theta = 20°$, $P = 2$ μm, and $D = 368$ nm. The simulations take into account the finite reflection loss due to the complex nature of the silver dielectric function. The field pattern observed in the cover layer is indicative of interference between the incident plane wave and the specularly reflected wave from the electrode surface. Fields transmitted through the electrode gap show amplitude variations along the lateral direction, indicative of the superposition of the incident plane wave with the high-angle reflected beam originating from the electrode surface. Figure 3(b) shows a snapshot of the magnetic field intensity H_y under TM illumination at the same wavelength. Similar field patterns are observed with the exception of a fine field pattern along the electrode surfaces resulting from the excitation of surface plasmon polaritons (SPP) on the silver electrode.

Figure 3(c) shows the simulated TE transmission, reflection, and absorption of the silver electrode structure. Many local transmission minima are observed due to diffractive effects, however, the frequency-averaged

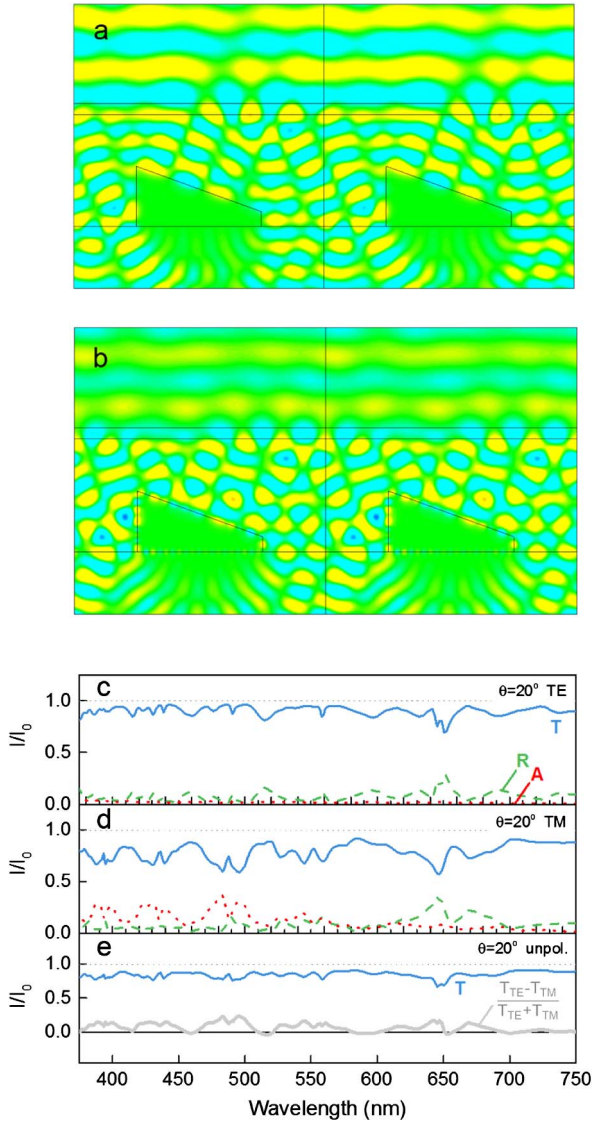

Fig. 3. (a) Electric field distribution under normal incidence TE illumination and (b) magnetic field distribution under TM illumination at $\lambda = 417$ nm of an interdigitated silver electrode on a substrate with refractive index $n = 2$, embedded in an index-matched layer covered with an 88 nm thick antireflection coating ($n = 1.41$) for a surface tilt of 20°, an electrode period of 2 μm, and a cover layer thickness of 368 nm. (c) Simulated TE transmission and (d) TM transmission (blue lines), reflection (green lines), and absorption (red lines) of the electrode. (e) Transmission of unpolarized light (blue line) and degree of polarization (gray line).

transmission over the entire wavelength range of 375–750 nm is 90%. The TM transmission [Fig. 3(d)] shows a frequency-averaged transmission of 77% across the same wavelength range. Figure 3(e) shows the corresponding transmission of unpolarized light (blue line), exhibiting a frequency-averaged transmission of 84%, a factor 1.7 higher than the expected transmission of 50% based on metal areal coverage. The degree of polarization $(T_{TE} - T_{TM})/(T_{TE} + T_{TM})$ is included (gray line) and is less than 24% across the full spectral range.

The presented approach is scale independent at large structure sizes but becomes less effective as electrode sizes approach the optical wavelength. At such small electrode dimensions specular reflection is no longer well-defined as diffractive effects begin to play an important role, while surface plasmon excitation may become a significant source of loss. To demonstrate how scaling of this design begins to breaks down at subwavelength feature sizes, the following discusses an aluminum electrode optimized for high transmission in the near-UV using an extremely small electrode gap of 75 nm and equal electrode width. Figure 4(a) shows a snapshot of the electric field distribution E_y under TE illumination at $\lambda = 250$ nm of a catoptric surface consisting of sculpted interdigitated aluminum [8] electrodes with an average thickness of 25 nm on a substrate with $n = 2$ embedded in an index-matched layer covered with an antireflection coating ($n = 1.41$, thickness 44 nm). The geometrical parameters are $\theta = 20°$, $P = 150$ nm, and $D = 31$ nm corresponding to the previously discussed geometric optimum. The array is seen to generate a large field amplitude in the electrode gap, suggesting large optical transmission. Figure 4(b) shows the H_y component under TM illumination at this wavelength. In this case the electrodes are seen to support standing

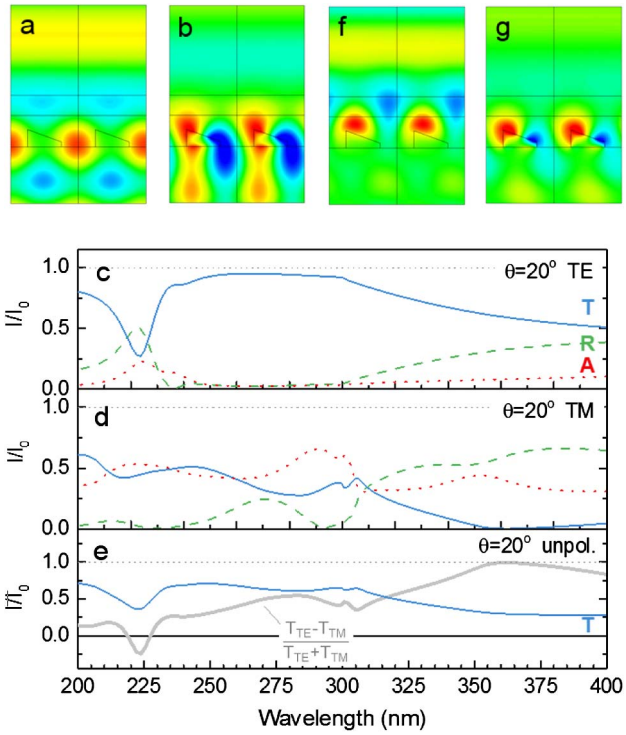

Fig. 4. Simulated light transmission through an aluminum catoptric electrode structure optimized for high transmission at ultraviolet wavelengths, showing (a) the electric field distribution under normal incidence TE illumination and (b) the magnetic field distribution under TM illumination at $\lambda = 250$ nm of an interdigitated rectangular aluminum electrode with a cross section of 75 nm × 25 nm, a periodicity of 150 nm, a cover layer thickness of 30 nm, and an antireflection coating with index $n = 1.41$ and thickness 44 nm. (c) Simulated TE transmission and (d) TM transmission (blue lines), reflection (green lines), and absorption (red lines) of the electrode. (e) Transmission of unpolarized light (blue line) and degree of polarization (gray line). (f) Electric field distribution under normal incidence TE illumination at $\lambda = 210$ nm, and (g) magnetic field distribution under TM illumination at $\lambda = 330$ nm.

SPP waves, as evidenced by the magnetic field maximum at the electrode–substrate interface. Figure 4(c) shows the calculated transmission, reflection, and absorption spectra of this structure under TE illumination. For wavelengths between 245 and 300 nm, transmission larger than 90% is achieved at the chosen 50% percent Al areal coverage. A reduction of the transmission is observed at wavelengths above 300 nm, coinciding with the cutoff wavelength for diffractive effects within the cover layer (condition $\lambda_0 \approx n_{\mathrm{cov}} \times P$) leading to increased reflection losses. This wavelength also corresponds to the cutoff wavelength of the 75 nm wide metal waveguide formed by the electrode gap, resulting in increased absorption for wavelengths above 300 nm. An additional transmission reduction is observed for wavelengths near 222 nm, close to the wavelength where the first (internal) diffracted order matches θ_{TIR} (condition $\lambda_0 = P$). The corresponding E_y distribution is shown in Fig. 4(f), revealing a guided mode in the cover layer with an antinode in the electrode gap, leading to low transmission. Figure 4(d) shows the transmission, absorption, and reflection under TM illumination. Transmission in excess of 50% is achieved at wavelengths between ~240 *and* 250 nm. Figure 4(g) shows the H_y distribution for TM illumination at the strong absorption peak at 290 nm, revealing large surface plasmon amplitude on the aluminum electrode, resulting in significant power dissipation. This observation indicates that the excitation of SPPs mediated by the sharp electrode corners becomes a significant loss contribution at small electrode sizes. The transmission spectrum of unpolarized light is shown in Fig. 4(e). The average transmission exceeds the 50% classical transmission limit of 227–320 nm, demonstrating that TIR-mediated light redirection remains feasible even at wavelengths and structure sizes outside the ray-optics regime.

In summary, a new embedded electrode design has been proposed that achieves close to perfect transmission at 50% metal coverage using a method that is approximately frequency and polarization independent for structures significantly larger than the optical wavelength. Any optical devices that utilize densely spaced top metal contacts while requiring large optical transmission may benefit from the presented approach. While the shown examples focused on electrode surfaces with a single tilt angle and a fixed 50% metal coverage, the metal surfaces may be shaped to optimize the transmission at even larger metal areal coverage. The general applicability of the approach, the broadband nature of the basic operating principle, and the simplicity of the design make this approach a promising candidate for high-transmission electrodes on a broad range of optical devices operating at wavelengths ranging from the ultraviolet to the infrared.

References

1. C. Genet and T. W. Ebbesen, Nature **445**, 39 (2007).
2. L. Martin-Moreno, F. J. Garcia-Vidal, H. J. Lezec, K. M. Pellerin, T. Thio, J. B. Pendry, and T. W. Ebbesen, Phys. Rev. Lett. **86**, 1114 (2001).
3. S. J. Lee, Z. Y. Ku, A. Barve, J. Montoya, W. Y. Jang, S. R. J. Brueck, M. Sundaram, A. Reisinger, S. Krishna, and S. K. Noh, Nat. Commun. **2**, 286 (2011).
4. A. Alu, G. D'Aguanno, N. Mattiucci, and M. J. Bloemer, Phys. Rev. Lett. **106**, 123902 (2011).
5. C. Argyropoulos, G. D'Aguanno, N. Mattiucci, N. Akozbek, M. J. Bloemer, and A. Alu, Phys. Rev. B **85**, 024304 (2012).
6. K. Q. Le, C. Argyropoulos, N. Mattiucci, G. D'Aguanno, M. J. Bloemer, and A. Alu, J. Appl. Phys. **112**, 094317 (2012).
7. P. B. Johnson and R. W. Christy, Phys. Rev. B **6**, 4370 (1972).
8. E. D. Palik and G. Ghosh, *Handbook of Optical Constants of Solids* (Academic, 1985).